IEEE Photonics Journal
An IEEE Photonics Society Publication

Open Access

Experimental Observation of Dynamic Transmission Lineshapes in a Robust SNAP Microbottle-Taper Coupling System

Volume 11, Number 6, December 2019

Mengyu Wang
Sifan Zeng
Lingjun Meng
Yu Yang
Xueying Jin
Yongchao Dong
Lei Zhang
Wenbin Xu
Keyi Wang

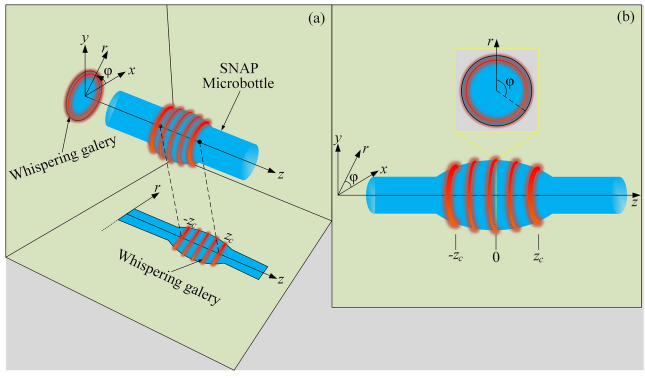

DOI: 10.1109/JPHOT.2019.2948300

Experimental Observation of Dynamic Transmission Lineshapes in a Robust SNAP Microbottle-Taper Coupling System

Mengyu Wang,[1] Sifan Zeng,[2] Lingjun Meng,[1] Yu Yang,[1] Xueying Jin,[3] Yongchao Dong,[4] Lei Zhang,[1] Wenbin Xu,[5] and Keyi Wang[1]

[1]Department of Precision and Precision Instrumentation, University of Science and Technology of China, Hefei 230026, China
[2]Department of Engineering and Applied Physics, University of Science and Technology of China, Hefei 230026, China
[3]School of Instrument Science and Technology, Hefei University of Technology, Hefei 230009, China
[4]School of Electromechanical Engineering, Guangdong University of Technology, Guangzhou 510643, China
[5]Science and Technology on Optical Radiation Laboratory, Beijing 100039, China

DOI:10.1109/JPHOT.2019.2948300

Manuscript received August 25, 2019; revised October 4, 2019; accepted October 15, 2019. Date of publication October 25, 2019; date of current version December 13, 2019. This work was supported in part by the National Natural Science Foundation of China under Grants 61775209, 61801129, 41871229, 61275011 and in part by the Fundamental Research Funds for the Central Universities JZ2019HGTA0050, JZ2019HGBZ0122. *(Mengyu Wang and Sifan Zeng contributed equally to this work.)* Corresponding authors: Lei Zhang; Keyi Wang (e-mail: lzhlzh@ustc.edu.cn; kywang@ustc.edu.cn.)

Abstract: Fano-like lineshapes in whispering-gallery modes (WGMs) microresonators are of critical for many actual applications, such as high-sensitivity sensors, slow light, and optical switches. In this paper, we theoretically and experimentally demonstrate dynamic transmission lineshapes, including Lorentzian lineshapes, Fano-like lineshapes and gain-like lineshapes, with a simple system, where a surface nanoscale axial photonic (SNAP) microbottle is coupled to the transition of a tapered fiber by carefully choosing tapered fiber diameters. Controlled and robust coupling with a clean and almost equidistant spectrum for different axial modes is achieved while maintaining contact between the resonator and the taper. Our device offers five similar dynamic transmission lineshapes arranged in order simultaneously, demonstrating stable tuning and a high number of potential degrees of freedom in contrast to other coupling systems for single- or double-coupled microresonators. By using coupled-mode theory, these transmission lineshapes are fitted to explain these experiment observations. We also explore a tunable transmission spectra obtained by increasing the powers of the input laser. Our approach hold unique potential in sensitivity-enhanced sensing, quantum information processing, and all-optical switching.

Index Terms: Microresonators, whispering-gallery mode, Fano-like resonance, transmission lineshapes.

1. Introduction

The transmission lineshapes, including Lorentzian lineshapes, especially Fano-like lineshapes, have attracted considerable research interests in the past decades due to their unique characteristics [1]. In particular, the realization of Fano-like lineshapes makes a step forward for improved

optical switching [2], nonlinear effects [3], slope sensitivity enhancement [4], and optical signal processing [5]. Classic all-optical analogies to Fano-like resonance have been realized in various configurations of coupled resonators, including self-coupled optical waveguide resonator [6], photonic crystal microcavities [7], plasmonic nanostructures [8], and optical microresonator [4], [9]–[13]. Specifically, optical microresonators supporting whispering-gallery modes (WGMs) have a good performance because of the advantages of compact structure, high quality (Q) factors and low mode volumes.

Unlike a conventional Lorentz resonance with a symmetric lineshape, Fano-like resonance has an asymmetric line shape, which is ascribed to the interference between a discrete localized state and a continuum state [1]. Interference between the resonant and a background scattering is the mechanism for these dynamical lineshapes using different tuning methods. Chiba *et al.* firstly investigated Fano-like lineshapes in a multimode tapered fiber coupled with a microsphere resonator [9]. However, the intensity of background light in directly transmission is so weak that the slope of these Fano-like lineshapes are low. Tomita *et al.* introduced a sharp asymmetric Fano-like lineshapes, resulting from the interference effect caused by two microsphere resonators by thermal tuning [10]. Recently, sharp Fano-like lineshapes and gain-like lineshapes have been achieved by various methods, including changing the coupling gap [11], mechanical [12], and pressure [13]. However, these tuning methods strongly depend on the coupling condition and the displacement precisely controlled by a nano translation stage. More recently, Liao *et al.* demonstrated coupling of a deteriorated mode with a high-Q WGM generates asymmetric Fano-like lineshapes, which was used to enhance the detection sensitivity of sensing device by 4.3 times [4]. However, the resonance transmission spectra were irregular even through the cleaned-up spectrum has been achieved by introducing a loss element of ultraviolet curable adhesive to selectively suppress the modes in the microresonator. In addition, these dynamical lineshapes have only achieved single dynamic transmission lineshapes, which is a drawback in terms of tuning and degree-of-freedom limitations.

In this paper, we report dynamic transmission lineshapes that can be changed from Lorentzian lineshapes to Fano-like lineshapes (and back) in the compact microbottle resonator with surface nanoscale axial photonics (SNAP) structure, which was firstly put forward and demonstrated in [14], [15]. Controlled and robust coupling with a clean and almost equidistant spectrum for different axial modes is achieved. The dynamic transmission lineshapes are experimentally achieved by selecting different coupling positions and theoretically analyzed using the coupled-mode theory, where different lineshapes result from the interference between the fundamental mode and higher order modes of the taper that are coupled to the WGMs of the resonator. In particular, our device in the SNAP microbottle-taper coupling system provides mechanical stability while maintaining contact between the resonator and the tapered fiber. In addition, three-dimensional WGMs in our SNAP microbottles are reported by full-scale wave equation calculation. Moreover, the resonant wavelength can be shifted significantly by increasing the power of the input laser.

2. Mode Characteristic and Theoretical Model

2.1 Mode Characteristic

Fig. 1(a) and (b) illustrate the 3D and 2D schematics of the WGMs in our SNAP microbottle resonator in the orthogonal curvilinear coordinates (z, r, φ). In combination with equatorial modes and bottle modes [16], microbottle resonators [17] exhibits a richer spectrum compared to other standard equatorial WGM microresonators [14]–[19]. Previously, Sumersky has calculated the eigen-frequency at the steady state using the stationary Schrödinger equation to describe the propagation of the WGMs in such a resonator [15]. To depict the SNAP microbottle configuration, a truncated harmonic-oscillator equation can be considered to attain an approximate parabolic profile along the z-axis to describe its profile $r(z) = (R_0 + \Delta r_0)[1 - 1/2(\Delta k z)^2]$, where z is the resonator axis direction, $R_0 + \Delta r_0$ is the radius at $z = 0$, and Δk is the curvature of the microbottle profile [14]–[19]. Three quantum indices (m, p, q) are characterized to describe the modes in our res-

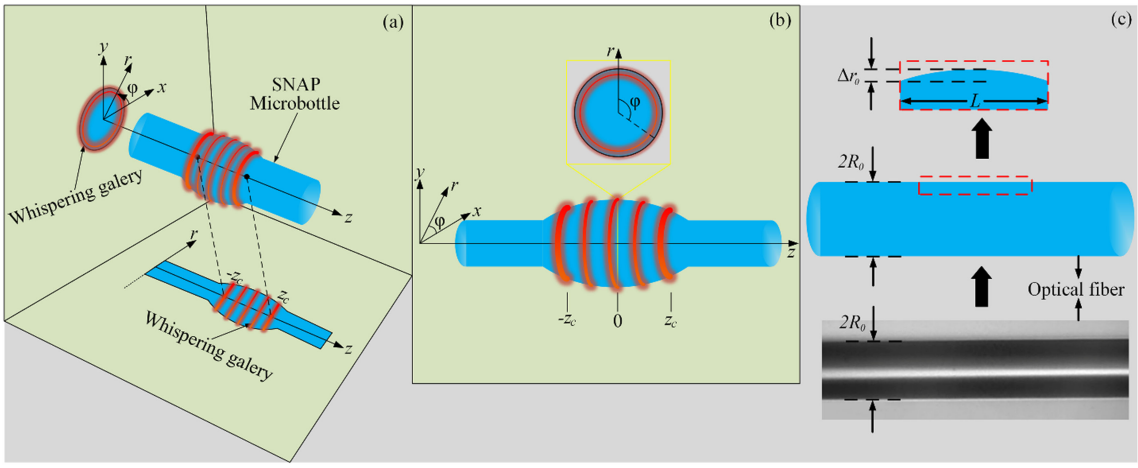

Fig. 1. (a) Three-dimensional diagram of WGMs in SNAP microbottle resonator in the orthogonal curvilinear coordinates (z, r, φ). (b) Two-dimensional diagram of WGMs action in SNAP microbottle resonator on the plane (z, φ) with a cutaway view of the plane (r, φ). Excited WGMs in the resonator are shown in red between turning points, $-z_c$ and z_c. (c) Schematic of a SNAP microbottle resonator fabricated via arc discharge. The diameter of optical fiber is $2R_0$, and the axial length of the resonator is L with a radius variation Δr_0.

onator: m represents the orders of the angular mode, p represents those of the radial mode, and q represents those of the axial mode [18], [19].

In the case of bottle symmetry, the optical field distribution in the resonator is given by separated wave equation

$$(\nabla^2 + k^2)\Delta\Phi\left(r, R\left(z\right)\right) Z\left(z\right) e^{jm\varphi} = 0 \tag{1}$$

The radial field distribution is written as [19]

$$\Phi_{m,p}\left(r, z\right) = \begin{cases} A_m J_m\left(k_0 n_1 R_c \Delta r / R\left(z\right)\right) & r \le R\left(z\right) \\ B_m Y_m\left(k_0 n_0 R_c \Delta r / R\left(z\right)\right) & r > R\left(z\right) \end{cases} \tag{2}$$

where J_m and Y_m denote the Bessel function and Hankel function, respectively. The constants A_m and B_m are determined by the boundary conditions. $R_c = R(z_c)$ and $-z_c \le z \le z_c$, $k_0 = 2\pi n_1/\lambda_0$. In the studied case, the axial field distribution can be expressed as [18], [19]

$$Z_{m,q}\left(z\right) = C_{m,q} H_q\left(\sqrt{\Delta E_m/2}\Delta z\right) \exp\left(-\Delta E_m \Delta z^2/4\right) \tag{3}$$

where H_q is the qth-order Hermite polynomial, the normalization $C_{m,q} = [\Delta E_m/\pi 2^{2q+1}(q!)^2]^{1/4}$, and $\Delta E_m = 2m\Delta k/(c_r R_0)$ with the correction factor $c_r = 0.957$ calculated from the axial intensity distribution of the TM polarized $q = 0$ mode. In the scalar approximation, the field distribution in the 3D SNAP microbottle is expressed as

$$E_{m,p,q}\left(r, z\right) = \Phi_{m,p}\left(r, z\right) \Delta Z_{m,q}\left(z\right) \Delta e^{jm\varphi} \tag{4}$$

Moreover, the resonant wavelength for each mode is given by [19]

$$\lambda_{m,q} = 2\pi n_1 \left(\left(\frac{m}{c_r\left(R_0 + \Delta r_0\right)} \right)^2 + \left(q + \frac{1}{2} \right) \Delta E_m \right)^{-1/2} \tag{5}$$

The axial spreading of each mode, defined by the corresponding turning point, can be given by [19]

$$z_c = \left(\frac{4}{\Delta E_m}\left(q+\frac{1}{2}\right)\right)^{-1/2} \tag{6}$$

Depending on their shape, light in the microbottle resonator is localized between two turning points, with an enhanced field strength at two well-separated spatial regions on the order of a few micrometers. Beyond this, the optical mode is evanescent. The SNAP resonator was fabricated by heating a single-mode fiber with a diameter of 125 μm via arc discharge with a standard fusion splicer, as shown Fig. 1(c).

2.2 Coupled-Mode Theory

The WGMs guide the optical light inside the SNAP microbottle and circulates about the surface of the resonator by continuous total internal reflection, leading to a high *Q*-factor being achieved. However, the light in the WGMs is strongly confined. The tapered fiber waveguide is an effective method for achieving evanescent coupling [20]. Here, the tapered fiber, whose waist was significantly thinned, was made by the heat-and-pull technique. We fabricated a tapered fiber with a waist diameter of about $d_t = 2.4$ μm over a length of about 2.5 mm. The length was important in our case as we must approach a dynamic transmission lineshapes. The benefits of the tapered fiber are that it allows not only the alignment and focusing of the input light but also the effective collection of output light. The tapered fiber also allows for the easy integration of the resonator-tapered coupling system with other fiber optical systems easily because the tapered fibers are basically just modified optical fibers.

To describe the dynamic transmission lineshapes in the SNAP microbottle-taper coupling system, we then model the tapered fiber as a multimode waveguide in the near-waist region as shown in Fig. 3(b). For simplicity, if only two fiber modes, which are the fundamental mode (fiber mode 1) and the high-order mode (fiber mode 2), are considered to couple with one WGM in our resonator, there exists a phase shift $\Delta\varphi_0$ that causes the Fano-like and gain-like lineshapes. By using the coupled-mode theory [21], we can express the dynamic field inside the SNAP microbottle resonator as

$$\frac{da}{dt} = -\left(i\sigma + \frac{\kappa_0 + \kappa_{ex1} + \kappa_{ex2}}{2}\right)a + \sqrt{\kappa_{ex1}}E_1 + \sqrt{\kappa_{ex2}}e^{j\Delta\varphi_0}E_2 \tag{7}$$

where $\sigma = w - w_0$ designates the frequency detuning between the input light and the resonant frequency, and a is the amplitude of the WGM. κ_0 and κ_{ex1} (κ_{ex2}) denotes the intrinsic decay rate and external coupling decay rate for fiber mode 1 (mode 2), respectively. E_1 (E_2) is the input amplitude of mode 1 (mode 2). In this case, only mode 1 can be detected at the output $E_{out} = E_1 - \sqrt{\kappa_{ex1}}a$. The transmission normalized with the steady state can be given by

$$T = \left|\frac{i\sigma + \dfrac{\kappa_0 - \kappa_{ex1} + \kappa_{ex2}}{2} - \sqrt{\kappa_{ex1}}\sqrt{\kappa_{ex2}}e^{j\Delta\varphi_0}\Delta N}{i\sigma + \dfrac{\kappa_0 + \kappa_{ex1} + \kappa_{ex2}}{2}}\right|^2 \tag{8}$$

where $N = E_2/E_1$. This equation shows that the phase shift $\Delta\varphi_0$ characterizes the degree of asymmetry, hence, dominates the lineshape variation, and the field distribution ratio N determines the maximum degree of asymmetry.

The Fano-like and gain-like lineshapes results from the interference between two related discrete states (a single WGM excited by two fiber modes) and a continuum (fiber mode 1), analogized to the classical Fano-like and gain-like lineshape mechanism. The transmission T varies as a function of $\Delta\varphi_0$ and E_2/E_1 by giving the values of these parameters κ_0, κ_{ex1}, and κ_{ex2}. As shown in Fig. 2(c), it is seen that, the lineshape exhibits a symmetric Lorentz lineshape, which can be tuned to a Fano-like lineshape and a gain-like lineshape by modifying the different $\Delta\varphi_0$. Moreover, a larger N leads to

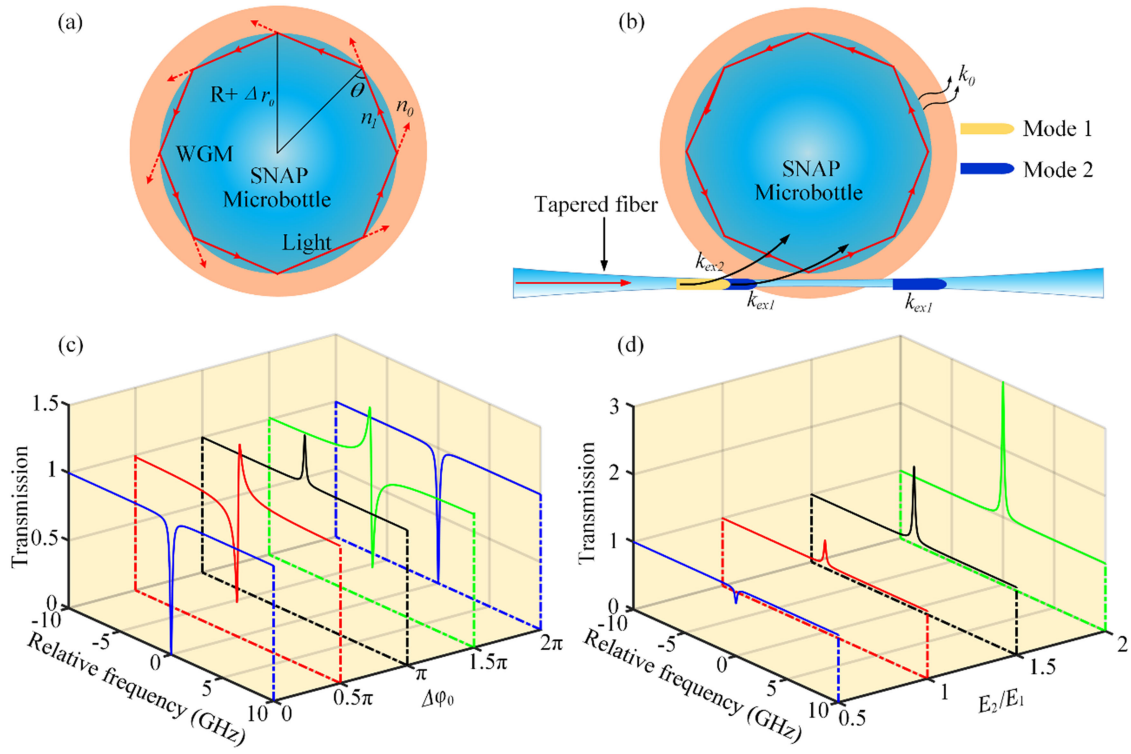

Fig. 2. (a) Geometric schematic of whispering-gallery modes in the SNAP microbottle resonator. Light trapping in the resonator by continuous TIR. $2R + 2\Delta r_0$ is the resonator diameter, n_1 and n_0 are the RI of the resonator and the surrounding medium. (b) Schematic of the dynamic transmission lineshapes generation in a SNAP microbottle-taper coupling system: Two fiber modes coupled with one WGM. Fig. 4. (a)–(b) Four kinds of transmission lineshapes with different phase shifts $\Delta\varphi_0$. Other parameters are set: $\kappa_0 = 2\kappa_{ex1} = 2\kappa_{ex2}$, $E_2/E_1 = 1$. (c)–(d) Four kinds of transmission lineshapes with different distribution radio E_2/E_1. Other parameters are set: $\kappa_0 = 2\kappa_{ex1} = \kappa_{ex2}$, $\Delta\varphi_0 = \pi$.

a stronger Fano and gain-like resonance as shown in Fig. 2(d). As the introduction of the input amplitude of mode 2 (E_2), the output transmission may become more than 1. As a result, the loss will become a gain in the microbottle. It is obvious that when $\Delta\varphi_0$ is an even-numbered multiple of π, the output transmission behaves a symmetric Lorentzian lineshape. In other cases, the lineshape behaves an asymmetric gain-like lineshape, especially when $\Delta\varphi_0$ is an odd-numbered multiple of π, the output transmission shows a symmetric gain-like lineshape. It should be noted that the phase shift $\Delta\varphi_0$ results in the periodical transmission lineshape, and the intensity distribution ratio N decides the maximum degree of asymmetry. Therefore, the two factors [N, $\Delta\varphi_0$] can be used to fit the experimental lineshapes. Thus, we will now provide a simple and effective method for dynamic transmission lineshape generation that can be changed from Lorentzian lineshapes to Fano-like lineshapes (and back) in our coupling system.

3. Experimental Setup and Results

3.1 Experimental Setup

In experiments, to characterize the transmission properties of our resonator, the resonance transmission spectrum was measured by coupling the photons of the tapered fiber to the resonator with help from the measurement setup in Fig. 3(a). A tunable diode laser in the 1550-nm wavelength band (Newfocus TLB 6728) controlled by a function generator was scanned to precisely excited WGMs in the resonator. Specifically, we applied a triangular wave signal with a period of 50 ms

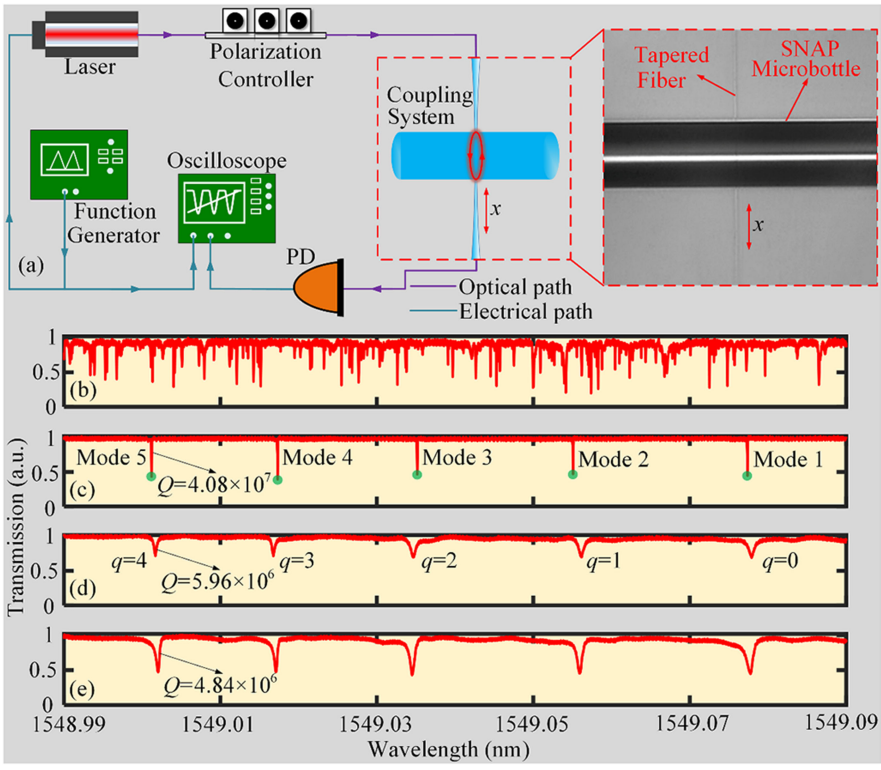

Fig. 3. (a) Experimental setup for measuring transmission properties of SNAP microbottle resonator. Inset: Micrograph of the SNAP microbottle coupled by a tapered fiber. (b) Transmission spectra for one typical microbottle resonator. (c) Transmission spectra for a particular gap distance between our SNAP microbottle resonator and the tapered fiber ($g = 500$ μm, $\Delta x = 0$ μm). (d) Transmission spectra when microbottle resonator keep in contact with the tapered fiber ($g = 0$ μm, $\Delta x = 0$ μm). (e) Transmission spectra for moving the resonator along the axis direction of the tapered fiber ($g = 0$ μm, $\Delta x = 1$ μm).

and the scan range of –1.2 V to 1.2 V, allowing a wavelength scan range of 0.1 nm, to observe the fine spectrum excited by the WGMs in our resonator. The polarization state of the launched light was controlled to a TM mode via a polarization controller. The tapered fiber was attached to a 3D controlled stage that allowed the precise positioning of a fiber with respect to the resonator. We monitored the resonator and tapered fiber from the top view and side view by using two charge-coupled device cameras. Then, the output was detected by a photodetector (PD, Thorlabs, PDA 10CF-EC, 150 MHz bandwidth) and monitored with a high-resolution digital oscilloscope (Keysight MSOS604A, 6 GHz bandwidth 20 GSa/s).

Fig. 3(b) shows the transmission spectrum of one microbottle with a central diameter 168 nm and a length 250 μm, which was fabricated by splicing together two sections of standard single mode fibers with easy pretreatment on the fiber ends [21]. However, in combination with equatorial modes and bottle modes [16], [18], the microbottle exhibits a rich spectrum. A dense spectrum makes it identify and trace the modes in some application, like sensing. Fig. 3(c)–(e) display three kinds of typical transmission spectra between the resonator and the tapered fiber. It should be noted that the presented spectra are significantly clean and easily identifiable when scanning with the same bandwidth, which is different from the spectrum of the normal microbottle and previously reported spectra in the microbottle [19], [21] due to their shallower confinement.

The dynamical transmission lineshapes for our SNAP microbottle resonator are characterized in two perspectives. Firstly, it is widely acknowledged that the gap (g) distance between the resonator and the tapered fiber significantly affects the coupling strength between the WGMs in the SNAP microbottle and the propagating mode of the fiber waveguide. In the center of the tapered fiber

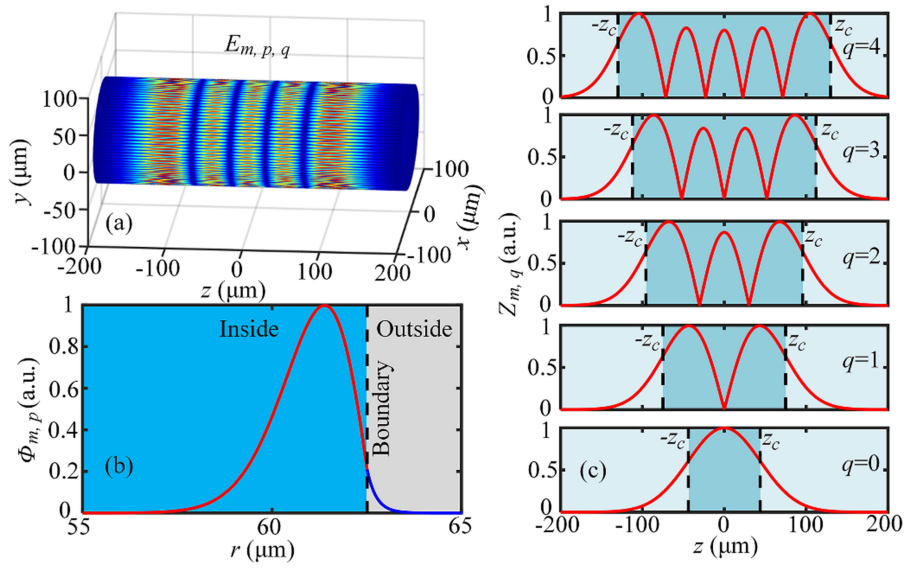

Fig. 4. (a) Three-dimensional normalized intensity distribution for the mode with $m = 356$, $p = 1$, and $q = 4$. (b) The normalized radial distribution for the mode with $m = 356$, $p = 1$ at $z = 0$. (c) Normalized axial field distributions for the modes with $m = 356$, $p = 1$, and $q = 0$-4. The horizontal black dashed lines indicate the positions of the turning points for the modes with $q = 0$-4.

($\Delta x = 0$ μm), to excite the WGMs efficiently, the dip depth was above 0.5 by a particular gap distance for $g = 500$ μm approximately, as shown in Fig. 3(c). It is evident that five modes, which are marked as modes 1 to 5 from right to left, are excited efficiently. To identify the spectrum, we theoretically calculated the resonant wavelengths as Eq. (5) and the modes distribution for the resonant wavelengths as Eq. (2)–(4). Thus, in our case, the diameter of our bottle is $2R_0 = 125$ μm with a radius variation $\Delta r_0 = 11$ nm, measured by the microfiber scanning method [21] (see Fig. 1(c) for its schematic diagram and experimental diagram). By setting these parameters: $n_1 = 1.467$, $n_0 = 1$, $m = 356$, $\Delta k = 0.88 \times 10^{-4}$ μm^{-1}, we found that the five modes correspond to the lowest five axial modes for $m = 356$, $p = 1$, and $q = 0$-4, whose resonant wavelengths are theoretically calculated as 1549.0803, 1549.0584, 1549.03366, 1549.0147, and 1548.9928 nm, respectively, as shown in Fig. 4. This resonance wavelengths shows a general agreement with our experimental results. The slight error comes from the asymmetric curvature of the nanoscale bump of our microbottle resonator. Fig. 4 presents the normalized intensity distribution for our SNAP microbottle resonator with an axial length of at least 400 μm. It can be clearly seen that the optical field is well-confined in the resonator.

Secondly, however, it is easy for the tapered fiber to make contact with the resonator ($g = 0$ μm) when it approaches close to the fiber because of electrostatic and van der Waals forces, leading to less overall absorption in the mode because of the low dip depth (just 0.3), as shown in Fig. 3(d). The phase matching can also be adjusted by choosing different fiber diameters along the taper axis direction. By vertically moving our resonator along the axis direction of the tapered fiber (x-direction) ($g = 0$ μm, $\Delta x = 1$ μm), efficient coupling can be achieved because of the result where the dip depth became above 0.5 again, as shown in Fig. 3(e). In this process, the tapered fiber waist is always in contact with the surface of the resonator. Especially, it provides a robust coupling and achieves a stable transmission spectrum. It is positioned perpendicular to the SNAP microbottle resonator and remains in physical contact during the experimental process, as mentioned in [15], [19], [23]–[25]. Therefore, the resonator is maintained in contact with the tapered fiber to enhance the robustness during the measurements. In contrast to the coupling gap tuning method reported elsewhere [10]–[13], this leads to a stable tuning process.

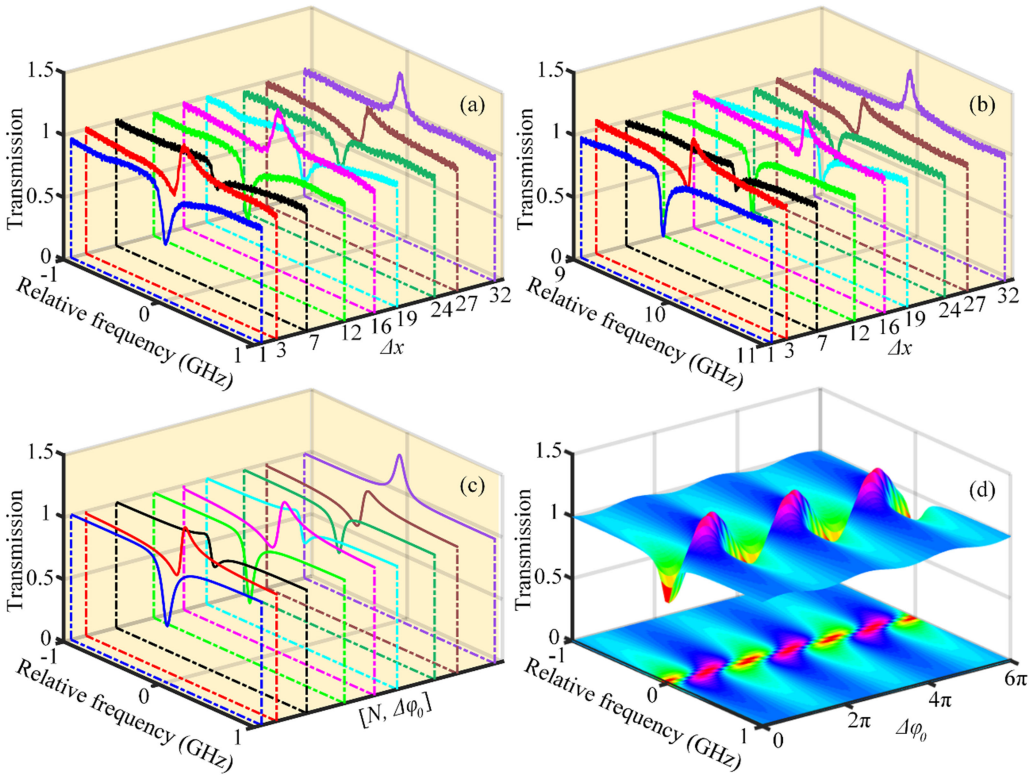

Fig. 5. Comparison between experimental lineshapes for (a) mode 1 and (b) mode 5 in Fig. 3. Normalized transmission spectra with nine different coupling positions Δx = 1, 3, 7, 12, 16, 19, 24, 27, and 32 μm, correspondingly. (c) Theoretical lineshapes for fitting these experimental lineshapes. Simulation parameters: $\kappa_0 = 0.0264$, $\kappa_{ex1} = 0.02 \cdot \kappa_0$, $\kappa_{ex2} = 2.5 \cdot \kappa_0$, $[N, \Delta\varphi_0] = [0.7,\ 0.25\pi]$, $[0.6,\ 0.395\pi]$, $[0.9,\ 1.395\pi]$, $[0.6,\ 2.1\pi]$, $[0.6,\ 2.355\pi]$, $[0.9,\ 3.395\pi]$, $[0.22,\ 3.9\pi]$, $[0.45,\ 4.35\pi]$, $[0.67,\ 5\pi]$. (d) Three-dimensional dynamic transmission lineshapes with completely different phase shifts $\Delta\varphi_0$.

Additionally, the axial wavelength FSR in our SNAP microbottle resonator, which is defined as the frequency spacing between modes with a fixed azimuthal quantum numbers *m*, and consecutive axial quantum numbers *q*, is about ~0.022 nm. The value of the axial of our resonator is about 190 times smaller than that of the azimuthal FSR for an equatorial microresonator of the same radius, which significantly reduces the tuning effort to over full FSR [26]. This facilitated their use in a large number of applications that require a resonant dip to coincide with a given frequency, such as sensing.

3.2 Dynamic Transmission Lineshapes

We next explored dynamic transmission lineshape generation by choosing the coupling position of the tapered fiber, as shown in Fig. 5. To achieve a stable tuning, the tapered fiber is maintained in constant contact with the surface of the resonator. These lineshapes start from the Lorentzian lineshapes, and converted to Fano lineshapes and then gain-like lineshapes when the chosen diameter of the tapered fiber increases. This lineshape evolution can be attributed to the fact that the phase shift and field distribution ratio between the two fiber modes depends on the coupling position. With the increasement in the taper diameter, the transmitted background increases in strength, which originates from the decrease in the insertion loss during the tuning process. Fig. 5(a) and (b) display normalized transmission spectra for the mode 1 and mode 5 from Fig. 3 measured at nine different coupling positions Δx = 1, 3, 7, 12, 16, 19, 24, 27, and 32 μm, correspondingly. The error of measurement was about 1 μm. Qualitatively, the two experimental transmission lineshapes

are similar. Fig. 5(c) reveals the dynamic lineshapes for mode 1 with the simulated results obtained using the theoretical model (Eq. (8)), where the correspondence between the coupling position of the tapered fiber and the value of $\Delta\varphi_0$ and N are given. The parameters calculated for the simulation are from these fitting data for the experimental results. The total process with the theoretical result is illustrated in Fig. 5(d). The experimental results are in good agreement with the theoretical results. Therefore, the theoretical model using coupled-mode theory is reasonable for explaining the dependence of the experimental dynamic transmission lineshapes generated by our SNAP microbottle-taper coupling system. It is evident that the phase shift between the two fiber modes $\Delta\varphi_0$ dominates the lineshape variation, which makes the spectra evolve periodically by 2π, while the field distribution ratio N determines the degree of asymmetry.

More specifically, it can be seen that as $\Delta\varphi_0$ increases from 0 to 2π, the lineshapes evolve from a Lorentzian; furthermore, it can be engineered Fano-like and gain-like lineshapes, by changing the distribution radio N; and finally, it returns to Lorentzian. These results is the same as the lineshapes when $\Delta\varphi_0$ increases from 2π to 4π and from 4π to 6π. In addition, it should be noted that with the decrease in the coupling diameter, the distribution ratio N increases. This further confirms the energy conversion between the two fiber modes in the tuning process. We found that the simulated lineshapes capture the major properties of the measured lineshapes. The slight deviation may be attributed to the involvement of other WGMs as well as the small variations in the coupling parameters when scanning the tapered fiber. It is found that some of the transmissions was altered, sometimes over 1. This phenomenon is due to the interaction between the evanescent fields in the microbottle and the tapered fiber. Furthermore, the transmission spectrum is the taper spectrum. It will slightly affect the shape of the tapered fiber when choosing tapered fiber diameters, thus leading to some of the transmissions being over 1.

It is important to point out that our experimental results indicate that the dynamic transmission spectra disappear and reappear periodically. The period is about 12 μm, which almost exceeds the periods reported in [9]. This phenomenon could be reproduced when scanning backward. The interesting phenomenon can be attributed to mode dispersion in the tapered fiber and can be theoretically explained by the multimode fiber waveguide coupled WGM model [19]. Theoretical analysis proves that the asymmetric Fano-like lineshape changes periodically with a period of $2\pi|\beta_1 - \beta_2|^{-1}$, where β_j ($j = 1, 2, \ldots$) refers to the propagation constants of the modes in the tapered fiber. For $d_t = 2.4$ μm ($\Delta x = 0$ μm), this permits the propagation of not only the fundamental propagation mode (HE_{11}, EH_{11}, TE_{01}, TM_{01}), but also some higher-order propagation modes, including HE_{21}, EH_{11}, and HE_{31} modes. Due to propagation constants of the HE_{11}, TE_{01}, HE_{21}, TM_{01}, EH_{11}, and HE_{31} modes at $d_t = 2.4$ μm, the calculated periods are 17.6 μm, 14.4 μm, 13.5 μm, 7.5 μm, and 5.9 μm for mode pairs HE_{11}/TE_{01}, HE_{11}/HE_{21}, HE_{11}/TM_{01}, HE_{11}/EH_{11}, and HE_{11}/HE_{31}, respectively. Note that the experimental period 12 μm is located between 13.5 μm and 7.5 μm, which indicates that the periodically varying Fano lineshapes observed in Fig. 5 can be attributed to the coupling HE_{11}, TM_{01}, and EH_{11} tapered modes and the WGMs. Propagation constant for these tapered modes are given in Fig. 6. HE_{11}, TM_{01}, and EH_{11} for the tapered diameters from 2.4 μm to 6 μm are calculated for comparison. Electric field distribution in cross section for some fiber guided modes at $d_t = 2.4$ μm has been inset by the finite element method in COMSOL in Fig. 6.

3.3 Thermal Tuning Transmission

Finally, we observe the transmission spectra dynamically tuned based on the thermo-optic effect. When the intensity of the input light is sufficiently big, a thermo-optic effect exists [27], [28]. In our case, the resonant wavelength of the SNAP microbottle resonator can be dynamically tuned by increasing the powers of the input laser. As show in Fig. 7, it is clear that, the resonant wavelength shifts about 560 pm when the pump current of the broadband light source increases from 66 mW to 186 mW with the help from an erbium-doped fiber amplifier. The relationship of the change in input current power and shift in the observed resonant wavelength is almost linear, and the corresponding sensitivity is about 4.66 pm/mW. Compared with previous works [28], our SNAP microbottle can operate in a wider wavelength range. In addition, since the thermal heating comes

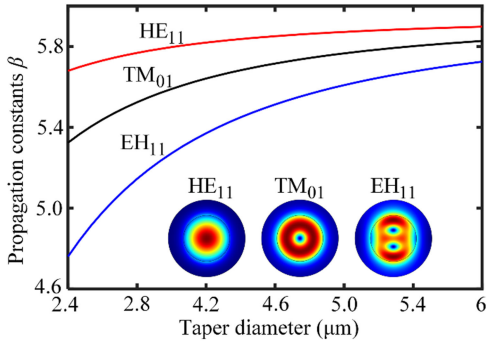

Fig. 6. Propagation constant of calculated mode (HE_{11}, TM_{01}, EH_{11}) for the tapered fiber as a function of the taper diameter. Inset: Electric field distribution in cross section for some fiber guided modes at $d_t = 2.4$ μm.

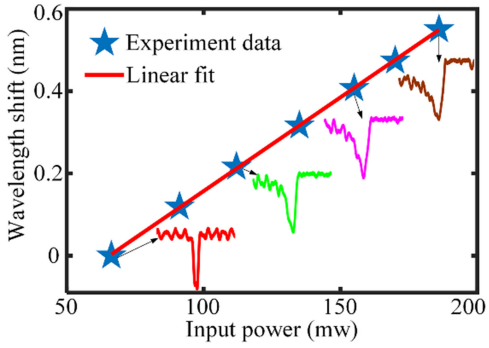

Fig. 7. Shift in resonant wavelength of the WGM peak as a function of the input light power. The red line is the linear fitting curve for the experimental data. The transmission spectra were obtained from the WGM peak with the increase in the input laser power.

from optical absorption, it increases with the input light power, leading to a broader resonant mode. The thermal-optic effect is very important to help us observe these physical phenomena in microresonators. In fact, it is because of the self-locking frequency phenomenon caused by the thermal effect that we can observe the rapidly varying dither signal caused by the photomechanical effect in the optical output spectrum [29]. Therefore, such a resonant-taper coupling structure provides a feasible approach to realize flexible dynamic transmission lineshapes. In such a case, the thermo-optic effect may be combined to together to enable a superior tuning performance.

3.4 Discussion

According to our results and analysis, the dynamic transmission lineshapes in our microbottle-taper coupling system naturally come with several advantages as summarized below: (a) The experimental spectra are demonstrated with a high Q-factor up to 4.08×10^7 and low axial FSR down to about 0.022 nm. Compared to the transmission lineshapes in coupled resonant system on SOI platform [26], our microbottle resonator exhibits a higher Q-factor. The results holds great potential in optical filters, sensors, nonlinear optics, and especially applications that require a resonant dip to coincide with a given frequency. (b) Controlled and robust coupling is realized in our SNAP microbottle-taper coupling system while maintaining contact between the resonators and the taper. Therefore, the tuning process is more immune to external perturbations such as air flow and tiny mechanical vibrations compared with the mechanical process reported in [10]–[13]. Compared with previously reported Fano resonances in a single microresonator system or double microresonator

system, the Fano-like resonance phenomenon is here more obvious and stable. (c) Our device in the robust coupling system offers five similar dynamic transmission lineshapes arranged in order simultaneously, demonstrating good performance in stable tuning and many degree-of-freedom possibilities in contrast to other coupling systems. In particular, our SNAP microbottle resonators presents a clean and almost equidistant transmission lineshapes with easily identifiable spectral features. (d) The experimental transmission spectra in our robust coupling system can also be tuned by some external methods, such as changing the input laser powers and environmental temperature.

4. Conclusions

In summary, we have theoretically and experimentally demonstrated a train of dynamic transmission lineshapes arranged in order. Transmission spectra are periodically observed because the Fano-like lineshapes can be obtained in a SNAP microbottle-taper coupling system. By vertically moving the tapered fiber, different Fano-like lineshapes are observed. This sharp Fano-like lineshape has great potential in optical switching and sensitivity-enhanced sensing. Our approach, realized in this work, offers a stable and fine platform for observation. The robust coupling system is used to investigate five dynamic transmission lineshapes arranged in order in contrast to other coupling systems for single- or double-coupled microresonators, demonstrating stable tuning and more degree-of-freedom possibilities. Our approach also explores tunable transmission spectra by increasing the powers of the input laser. The tunable lineshapes hold great potential in biochemical sensing, nonlinear effect and optical switching.

References

[1] A. E. Miroshnichenko, S. Flach, and Y. S. Kivshar, "Fano resonances in nanoscale structures," *Rev. Modern Phys.*, vol. 82, pp. 2257–2298, 2010.
[2] S. Fan, "Sharp asymmetric line shapes in side-coupled waveguidecavity systems," *Appl. Phys. Lett.*, vol. 80, pp. 908–910, 2002.
[3] M. Kroner *et al.*, "The nonlinear fano effect," *Nature*, vol. 451, pp. 311–314, 2008.
[4] J. Liao, X. Wu, L. Liu, and L. Xu, "Fano resonance and improved sensing performance in a spectral-simplified optofluidic micro-bubble resonator by introducing selective modal losses," *Opt. Exp.*, vol. 24, pp. 8574–8580, 2016.
[5] K. Totsuka, N. Kobayashi, and M. Tomita, "Slow light in coupled-resonator-induced transparency," *Phys. Rev. Lett.*, vol. 98, 2016, Art. no. 213904.
[6] L. Zhou, T. Ye, and J. Chen, "Coherent interference induced transparency in self-coupled optical waveguide-based resonators," *Opt. Lett.*, vol. 36, pp. 13–15, 2011.
[7] J. Pan *et al.*, "Tuning the coherent interaction in an on-chip photonic-crystal waveguide-resonator system," *Appl. Phys. Lett.*, vol. 97, 2010, Art. no. 101102.
[8] N. Liu *et al.*, "Plasmonic analogue of electromagnetically induced transparency at the Drude damping limit," *Nature Mater.*, vol. 8, pp. 758–762, 2009.
[9] A. Chiba, H. Fujiwara, J. Hotta, S. Takeuchi, and K. Sasaki, "Fano resonance in a multimode tapered fiber coupled with microspherical cavity," *Appl. Phys. Lett.*, vol. 86, 2005, Art. no. 261106.
[10] M. Tomita, K. Totsuka, R. Hanamura, and T. Matsumoto, "Tunable Fano interference effect in coupled-microsphere resonator-induced transparency," *J. Opt. Soc. Amer. B*, vol. 26, pp. 813–818, 2009.
[11] Y. Miao, Y. Peng, Y. Xiang, M. Li, Y. Lu, and Y. Song, "Dynamic Fano resonance in thin fiber taper coupled cylindrical microcavity," *IEEE Photon. J.*, vol. 8, no. 6, Dec. 2016, Art. no. 4502806.
[12] Y. Yang, S. Saurabh, J. Ward, and S. N. Chormaic, "Coupled-mode-induced transparency in aerostatically tuned microbubble whispering-gallery resonators," *Opt. Lett.*, vol. 40, pp. 1834–1837, 2015.
[13] Y. Wang, K. Zhang, S. Zhou, Y. Wu, M. Chi, and P. Hao, "Coupled-mode induced transparency in a bottle whispering-gallery-mode resonator," *Opt. Lett.*, vol. 41, pp. 1825–1828, 2016.
[14] M. Sumetsky *et al.*, "Surface nanoscale axial photonics: Robust fabrication of high-quality factor microresonators," *Opt. Lett.*, vol. 36, pp. 4824–4826, 2011.
[15] M. Sumetsky, "Theory of SNAP devices: Basic equations and comparison with the experiment," *Opt. Exp.*, vol. 20, pp. 22537–22554, 2012.
[16] M. Sumetsky, "Whispering-gallery-bottle microcavities: The three-dimensional etalon," *Opt. Lett.*, vol. 29, pp. 8–10, 2004.
[17] M. Sumetsky, "Optical bottle microresonators," *Prog. Quantum Electron.*, vol. 64, pp. 1–30, 2019.
[18] Y. Louyer, D. Meschede, and A. Rauschenbeutel, "Tunable whispering-gallery-mode resonators for cavity quantum electrodynamics," *Phys. Rev. A*, vol. 72, 2005, Art. no. 031801.
[19] G. S. Murugan, M. N. Petrovich, Y. Jung, J. S. Wilkinson, and M. N. Zervas, "Hollow-bottle optical microresonators," *Opt. Exp.*, vol. 19, pp. 20773–20784, 2011.

[20] M. Cai, O. Painter, and K. J. Vahala, "Observation of critical coupling in a fiber taper to a silica-microsphere whispering-gallery mode system," *Opt. Lett.*, vol. 85, pp. 74–77, 2000.
[21] K. Zhang, Y. Wang, and Y. H. Wu, "Enhanced Fano resonance in a non-adiabatic tapered fiber coupled with a microresonator," *Opt. Lett.*, vol. 42, pp. 2956–2959, 2017.
[22] Y. Dong, X. Jin, and K. Wang, "Selective excitation of high-Q resonant modes in a bottle/quasicylindrical microresonator," *Opt. Commun.*, vol. 372, pp. 106–112, 2016.
[23] F. Shen, X. Shu, L. Zhang, and M. Sumetsky, "Fabrication of surface nanoscale axial photonics structures with a femtosecond laser," *Opt. Lett.*, vol. 41, pp. 2795–2798, 2016.
[24] M. Sumetsky, K. Abedin, D. J. DiGiovanni, Y. Dulashko, J. M. Fini, and E. Monberg, "Coupled high Q-factor surface nanoscale axial photonics (SNAP) microresonators," *Opt. Lett.*, vol. 37, pp. 990–992, 2012.
[25] M. N. M. Nasir, G. S. Murugan, and M. N. Zervas, "Spectral cleaning and output modal transformations in whispering-gallery-mode microresonators," *J. Opt. Soc. Amer. B*, vol. 33, pp. 1963–1970, 2016.
[26] M. Sumetsky, Y. Dulashko, and R. S. Windeler, "Super free spectral range tunable optical microbubble resonator," *Opt. Lett.*, vol. 35, pp. 1866–1868, 2010.
[27] Z. Zhang *et al.*, "Experimental demonstration of thermally tunable Fano and EIT resonances in coupled resonant system on SOI platform," *IEEE Photon. J.*, vol. 10, no. 3, Jun. 2018, Art. no. 6601108.
[28] F. Bo *et al.*, "Lithium-niobate-silica hybrid whispering-gallery-mode resonators," *Adv. Mater.*, vol. 27, pp. 8075–8081, 2015.
[29] T. Carmon, L. Yang, and K. J. Vahla, "Dynamical thermal behavior and thermal self-stability of microcavities," *Opt. Exp.*, vol. 12, pp. 4742–4750, 2004.